ADVANCED ENERGY MATERIALS

Supporting Information

for *Adv. Energy Mater.,* DOI: 10.1002/aenm.202000310

Ion Migration-Induced Amorphization and Phase Segregation as a Degradation Mechanism in Planar Perovskite Solar Cells

Diego Di Girolamo, Nga Phung, Felix Utama Kosasih, Francesco Di Giacomo, Fabio Matteocci, Joel A. Smith, Marion A. Flatken, Hans Köbler, Silver H. Turren Cruz, Alessandro Mattoni, Lucio Cinà, Bernd Rech, Alessandro Latini, Giorgio Divitini, Caterina Ducati, Aldo Di Carlo, Danilo Dini,* and Antonio Abate**

Supporting Information for

Ion Migration-Induced Amorphization and Phase Segregation as a Degradation Mechanism in Planar Perovskite Solar Cells

Diego Di Girolamo,[§] Nga Phung,[§] Felix Utama Kosasih, Francesco Di Giacomo, Fabio Matteocci, Joel A. Smith, Marion A. Flatken, Hans Köbler, Silver H. Turren Cruz, Alessandro Mattoni, Lucio Cinà, Bernd Rech, Alessandro Latini, Giorgio Divitini, Caterina Ducati, Aldo Di Carlo, Danilo Dini,* and Antonio Abate**

[§]These authors contribute equally

Dr. D. Di Girolamo, Dr. A. Latini, Prof. D. Dini
Department of Chemistry
University of Rome "Sapienza"
Piazzale A. Moro 5, 00185 Rome, Italy
E-mail: danilo.dini@uniroma1.it

N. Phung, M. A. Flatken, H. Köbler, Dr. S. H. Turren Cruz, Prof. B. Rech Dr. A. Abate
Helmholtz-Zentrum Berlin für Materialien und Energie
Kekuléstraße 5, 12489 Berlin, Germany
E-mail: antonio.abate@helmholtz-berlin.de

F. U. Kosasih, Dr. G. Divitini, Prof. C. Ducati
Department of Materials Science and Metallurgy
University of Cambridge
27 Charles Babbage Road, Cambridge CB3 0FS, UK

Dr. D. Di Girolamo, Dr. A. Abate
Department of Chemical, Materials and Production Engineering
University of Naples Federico II
Piazzale Tecchio 80, 80125 Fuorigrotta, Naples, Italy
Email: antonio.abate@unina.it

Dr. F. Di Giacomo, Dr. F. Matteocci, Prof. A. Di Carlo
C.H.O.S.E. (Centre for Hybrid and Organic Solar Energy), Department of Electronic Engineering
University of Rome-Tor Vergata
Rome, 00133, Italy

Prof. A. Di Carlo
L.A.S.E – Laboratory of Advanced Solar Energy
National University of Science and Technology NUST-MISiS, Moscow, Russia.
E-mail: aldo.dicarlo@uniroma2.it

J. A. Smith.
Department of Physics and Astronomy
University of Sheffield
Sheffield, S3 7RH, UK

Dr. Alessandro Mattoni
Consiglio Nazionale delle Ricerche, Istituto Officina dei Materiali, CNR-IOM, Cagliari, Cittadella Universitaria, Monserrato 09042-I (CA), Italy

Dr. L. Cinà
CICCI Research, Piazzale Thailandia, 5 58100 Grosseto (GR) Italy

Prof. B. Rech
Faculty of Electrical Engineering and Computer Science, Technical University Berlin, Marchstraße 23, 10587 Berlin, Germany

SI Note 1

The choice of biasing potential deserves some discussion. Except for reverse biasing due to partial shadowing of modules, during its lifespan, a solar cell would stay most of the time at maximum point voltage (V_{MP}) in operation, or open circuit voltage (V_{OC}), if illuminated but not connected to an external load. Biasing around V_{OC}, therefore, appears to be a reasonable choice.[1] The NiO-based devices herein investigated generally yielded a V_{OC} in the range of 1.00 - 1.08 V (Figure SI1d), and the adoption of PTAA as the hole selective layer yielded 1.08 - 1.15 V (Figure SI1d). With the same CsFAMA composition, V_{OC} values above 1.2 V have been demonstrated when employing SnO_2 as the electron selective layer.[2] Further, by taking into account the band gap of the CsFAMA perovskite of 1.6 eV, the theoretical V_{OC} would be 1.3 V and the theoretical V_{MP} would be 1.2 V.[3] Therefore, a reasonable biasing potential should fall between 1.0 V and 1.3 V. Except when stated otherwise, we selected 1.2 V to conduct the experiments because it has already been attained as a V_{OC} value and thus represents a practical limit in this sense. Moreover, the current density at 1.2 V in the dark in our devices was of a similar magnitude to the short circuit current or current at maximum power point during photovoltaic operation. We remark that the dark current (whose injection is impossible to avoid in this context) flows in the opposite direction to the photo-current, which might bring different charge accumulation behavior or different electrochemistry with respect to the operating mechanism. However, the deconvolution of the degradation pathways induced by bias and light (along with the understanding of their combination) offers fundamental insights to understand how perovskite solar cells degrade. Finally, we remark that biasing at even higher potentials might be relevant for other applications, such as light-emitting diodes, and might deserve future investigation.

Figure SI1

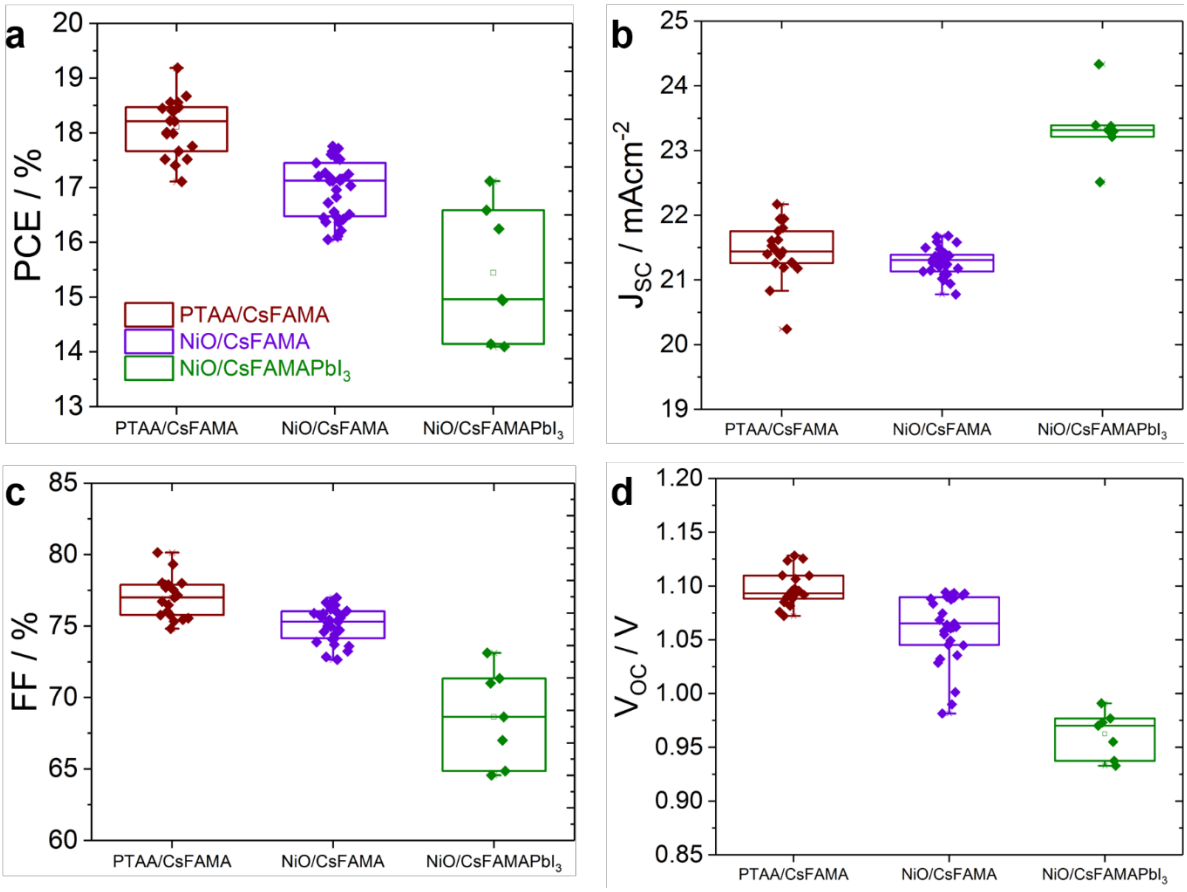

Photovoltaic performance statistics of devices employed in this study, obtained from reverse J-V scans at 100 mV/s with simulated AM1.5g spectrum: **a**. power conversion efficiency (PCE), **b**. short circuit current (J_{SC}), **c**.fill factor (FF), **d**. open circuit voltage (V_{OC}).

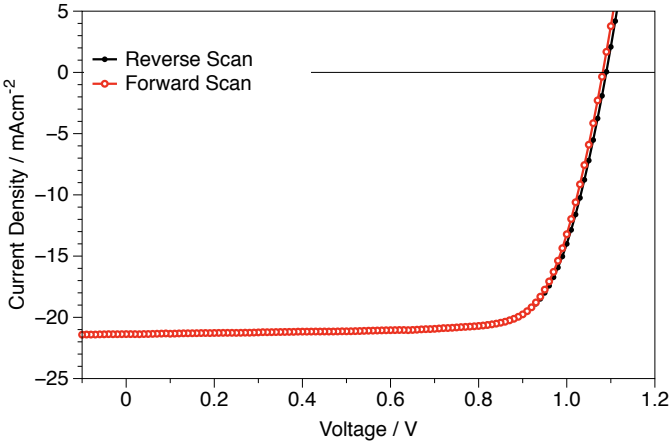

J-V scan of a typical NiO-based p-i-n PSC with negligible hysteresis.

Figure SI2

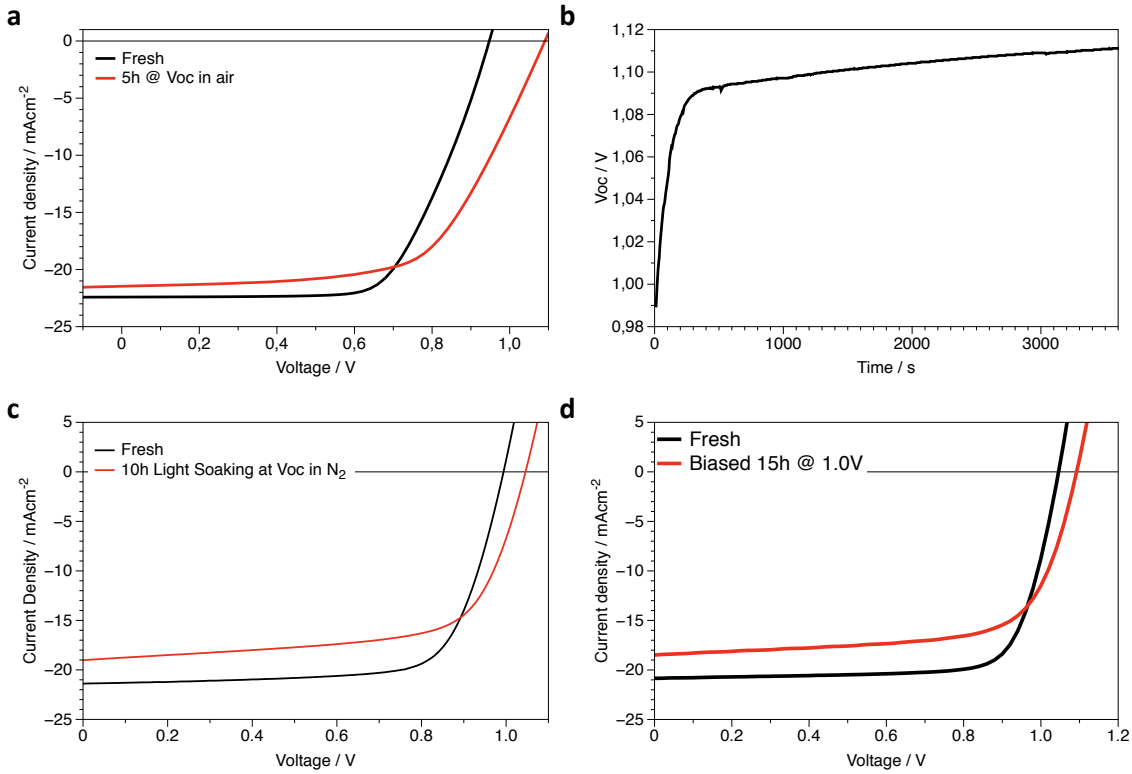

a J-V curve before (black) and after (red) a light soaking stress test in air. **b** 1h of V_{OC} rise in time. The V_{OC} remains stable after the plateau is attained. **c** J-V curve before (black) and after (red) a light soaking stress test in nitrogen. **d** The effect on the J-V curve of a prolonged (15h) bias at 1 V in dark. At this injected current, there is no halide segregation in CsFAMA mix halides device as can be seen from the electroluminescence measurement shown in figure 4d in the main text.

In Figure SI2, we report the results of a light soaking stress test performed in air (Figure SI2a) or in nitrogen (Figure SI2c) for an unencapsulated device. This preliminary test was performed to have a first insight into the practical implication of the mechanism we investigated in real photovoltaic conditions. Notably, the behavior of PV parameters was similar to what we observed with the stress discussed in this work: V_{OC} strongly increases, while J_{SC} and FF decrease. This result suggested that the ion migration driven mechanism we investigated might also be relevant in photovoltaic operation. Here, the V_{OC} was around 1.1 V for most of the time (see Figure SI2b, measured in air). Nonetheless, we wanted to stress that future investigations are required in order to understand in detail the overlapping effects of ion migration driven mechanisms with those caused by light and thermal induced degradation.

Figure SI3

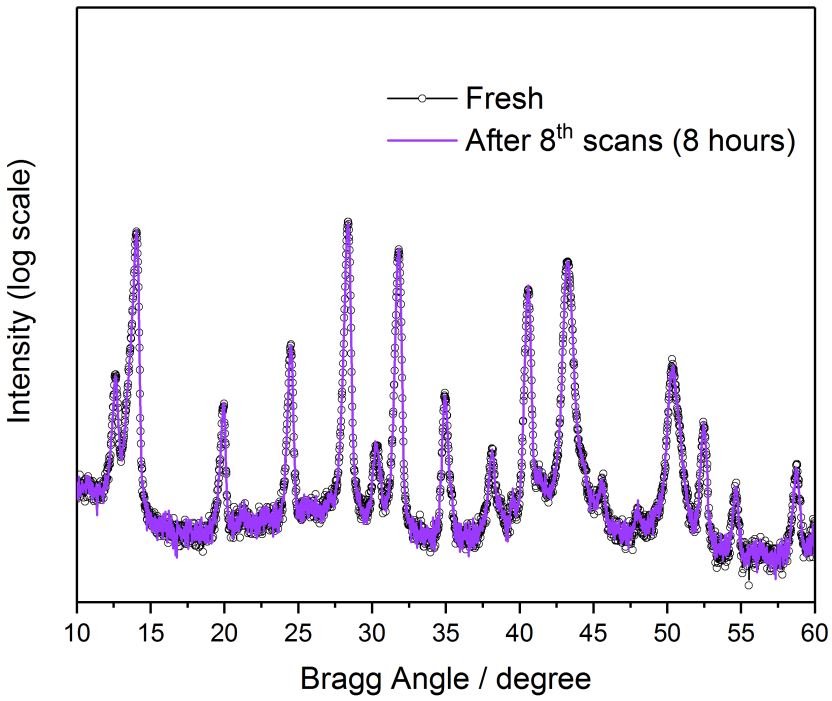

XRD patterns of a fresh sample and after 8 XRD scans (one scan per hour, without bias and otherwise similar conditions to the *in-situ* bias XRD measurement).

Figure SI4

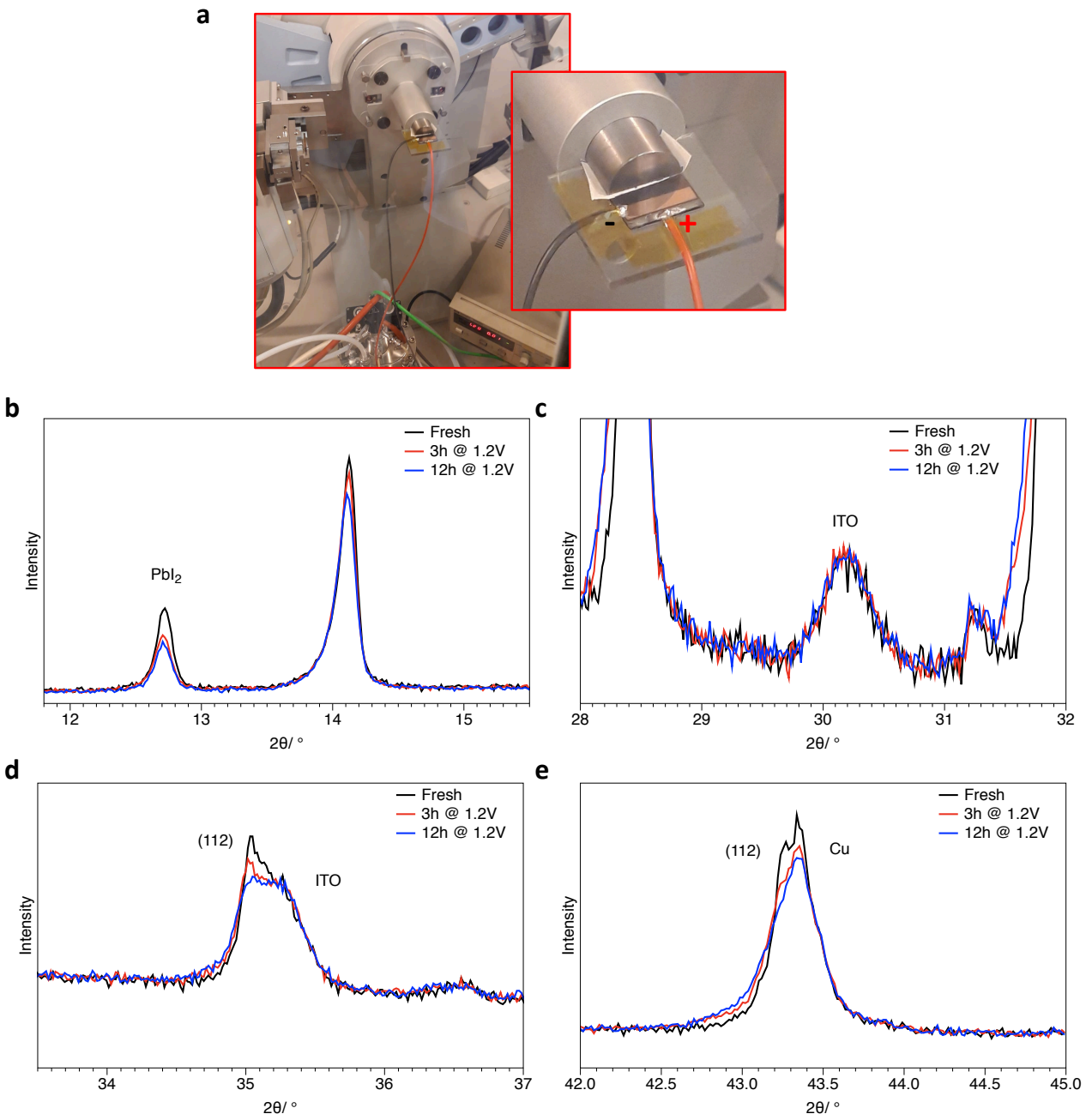

a Picture of the setup employed for the *in situ* XRD. The device (coincident with the copper stripe) is mounted on a glass holder by means of an adhesive tape. The contacts have been ultrasonically soldered to ensure higher mechanical stability and Kapton tape has been employed to fix the wires to the support to avoid any movement of the device over the whole experiment. The polarity of the contacts is specified in the magnification of the sample holder. The device is polarized at 1.2 V and about 10 mA are recorded by the source-meter, as it can be appreciated in the image. **b** Highlighting the PbI_2 XRD main peak at 12.7° and of the main perovskite peak at 14.1°. **c** Magnification on the ITO peak around 30°, which shows no variation of intensity and peak shape over the whole experiment. **d** Magnification of the feature around 35° which is composed of an overlapping peak from perovskite (at lower angles) and a peak from ITO (at higher angles), with the decrease in intensity completely attributable to the perovskite peak. **e** Magnification of the feature around 43°

which is composed of overlapping peaks from perovskite (at lower angles) and Cu (at higher angles), and again the decrease in intensity is attributable to the perovskite peak.

Figure SI5

Theoretical literature confirmed that highly mobile point defects could easily migrate[4] due to temperature and electric fields and indicated that defects easily accumulate at surfaces or interfaces[5]. The accumulation of point defects in a hybrid perovskite crystal induced a structural disorder and, at high concentration, it could also induce loss of the crystalline order and amorphization. This is shown in Figure SI5 where we report snapshots of molecular dynamics simulations of MAPI crystals[6] in presence of iodine interstitials at increasing concentration. Similar results were found for all kinds of defects (interstitial and vacancies) involving either cations or halogens. Amorphization was also observed in hybrid perovskites exposed to water.[7,8]

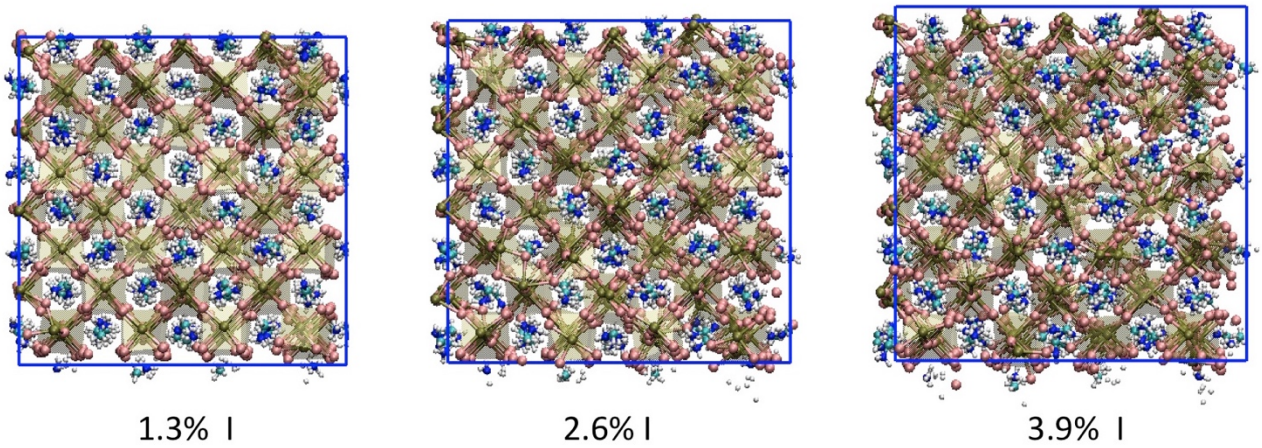

Snapshots of methylammonium lead iodide crystal (256 f.u.) containing iodine interstitials at increasing concentration simulated at 300 K by molecular dynamics. The concentration increases from left to right.

Figure SI6

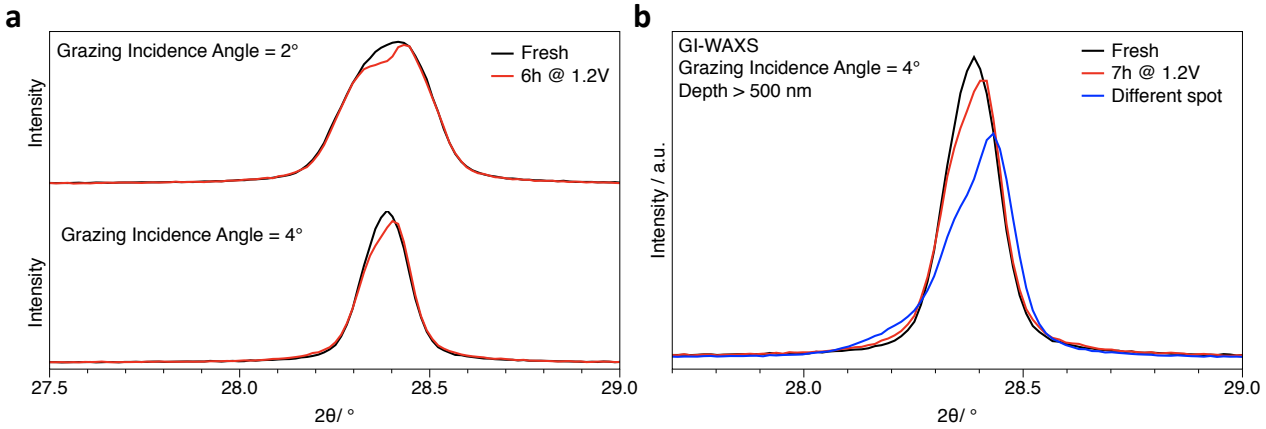

In-situ GIWAXS measurement pattern with focused at 28.4° peak for fresh samples and biased sample. **a** Difference in intensity reduction comparing the more surface (measurement at incidence angle of 2°) and through the whole perovskite layer (measurement at incidence angle of 4°). **b** The comparison with different spot after bias which indicates intensity reduction was not due to beam damage.

From the analysis on integrated intensity of *in situ* GIWAXS signal at 28.4° it was possible to estimate a higher degree of amorphization from the dataset collected with a grazing incidence angle of 2°, which was expected to be more surface sensitive. After about 5 hours of biasing, the integrated intensity drop was of about 1.2% when the grazing incidence angle was 4° and of about 4% when the grazing incidence angle was 2°. This fact supported the interfacial degradation mechanism we proposed, however, we refrained from using the quantitative analysis on this dataset because it appeared that the scattered signal intensity depended on the spot position across the pixel area (see Figure SI6b). This fact could arise from slight misalignments due to sample holder movement (changing the effective volume from which X-rays were scattered) or from non-uniformity in the degradation behavior over the device area.[9,10] As can be seen in Figure SI6b, the measurement at different spot next to the area, in which the beam hit during the in-situ measurement, confirmed that the beam damage could be neglected.

Figure SI7

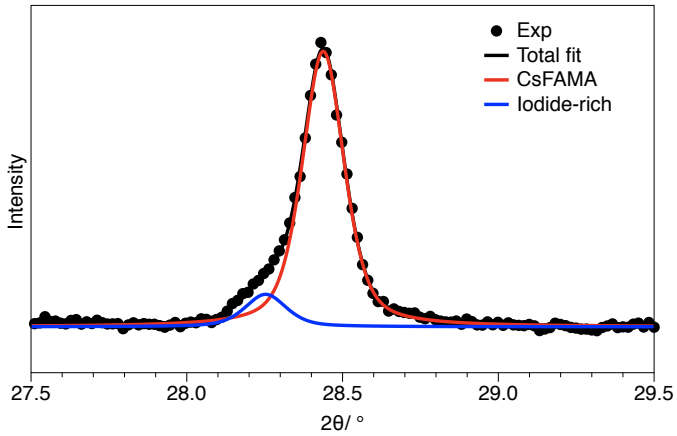

Fit employing two components for the XRD peak at 28.44° (a = 6.271 Å) after 3h of biasing.

The blue-component was at 28.25° (a = 6.313 Å) (estimated from Bragg's law assuming cubic crystal structure), and the positions of the two peaks were constant over the whole experiment. From the relative intensities of the fitted XRD peaks of the original CsFAMA and of the iodide-rich composition after 3h of biasing, we could estimate that about 10 vol% of the latter was enough to dominate light emission, with a detectable intense peak at 790 nm (Figure 2e), likely due to fast funneling to the low bandgap system.[11]

Figure SI8

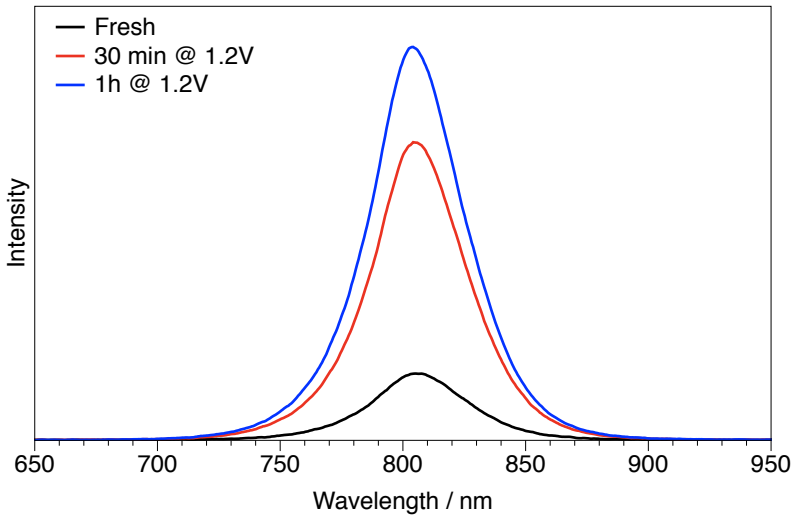

Electroluminescence (EL) spectrum evolution of $Cs_{0.05}(FA_{0.83}MA_{0.17})_{0.95}PbI_3$ perovskite upon biasing at 1.2 V in dark. The EL quantum efficiency (PL-QE) increases. The peak maximum for the fresh sample is at 805nm. After 1h at 1.2V the peak is found at 803.5nm.

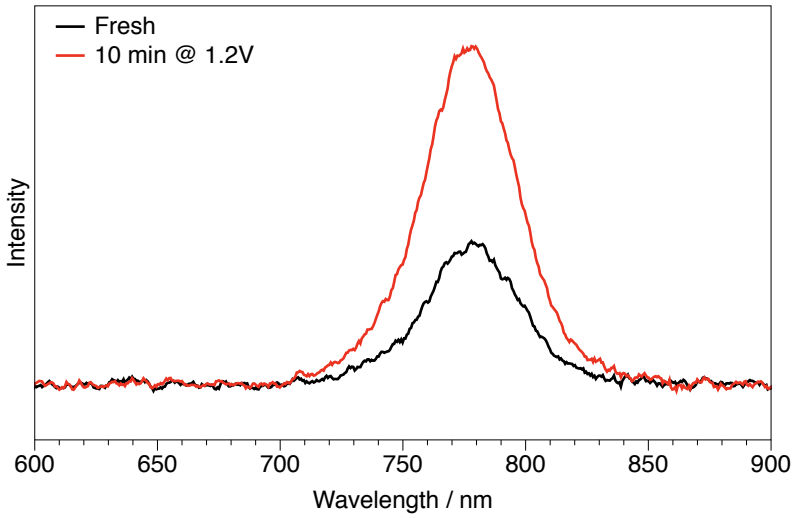

EL spectrum evolution of $MAPbI_3$ perovskite upon biasing at 1.2 V in dark. The EL-QE increases. The peak maximum for the fresh sample is at 779nm and at 777nm for the biased samples.

These two reference devices showed the absence of a shoulder appearance which pointed towards a stable composition different from a clear halide segregated phase evolution over time as can be seen in **Figure 2e**.

Figure SI9 NMF Analysis of STEM-EDX Data

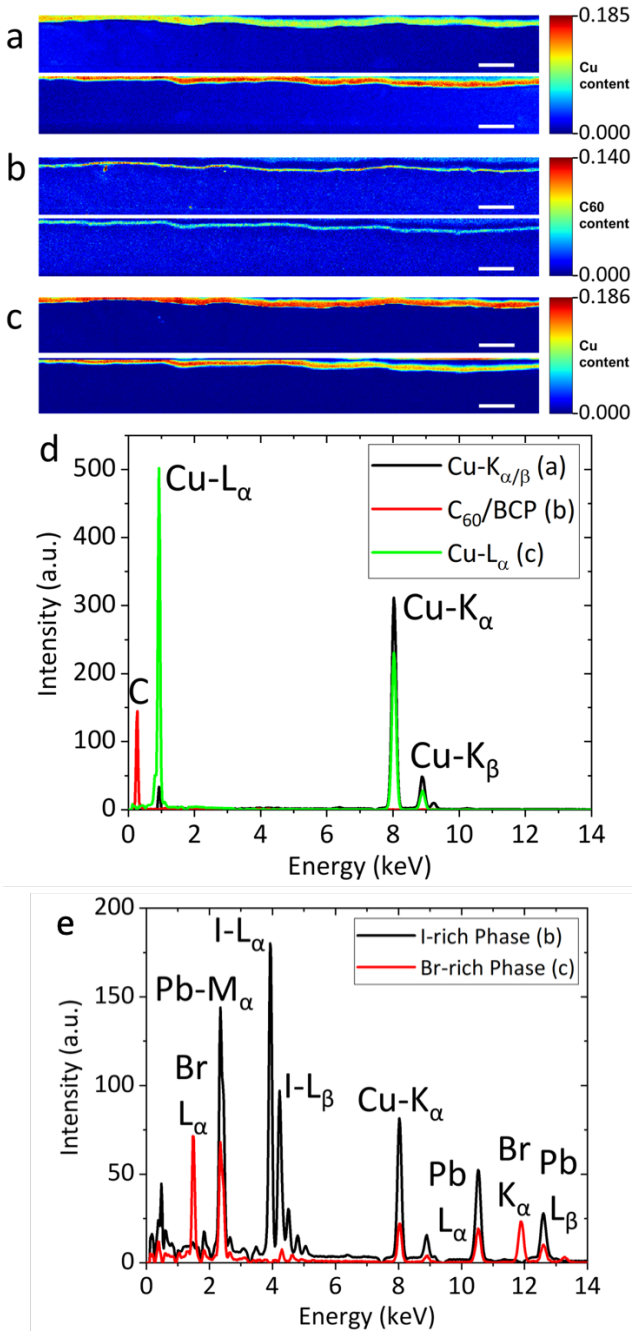

a-c NMF loadings (maps) of three selected components, with the fresh sample at the top and biased sample at the bottom of each pair: **a** copper electrode (Cu-$K_{\alpha/\beta}$ line), **b** C_{60}/BCP electron transport layer, and **c** copper electrode (Cu-L_{α} line). **d** NMF factors (spectra) of the loadings shown in (a-c). All scale bars are 0.5 µm. Numbers on the colour scale in (a-c) are in a.u. **d** NMF factors (spectra) of the loadings displayed in (Fig. 3b) and (Fig. 3c). The black spectrum contains iodide peaks, while the red one contains bromide peaks.

It can be seen from Figure 3 that the bromide rich phase formed aggregates in the both interfaces. This suggested that the potential drop at the interfaces played a vital role in halide redistribution. Moreover, as the bromide rich phase did not form a continuous layer at the interface, this indicated a contribution of the high dimensional crystallographic defects (*e.g.* grain boundaries) in defining and localizing the halide distribution after the bias which is in agreement with previous reports.[12,13]

Figure SI10

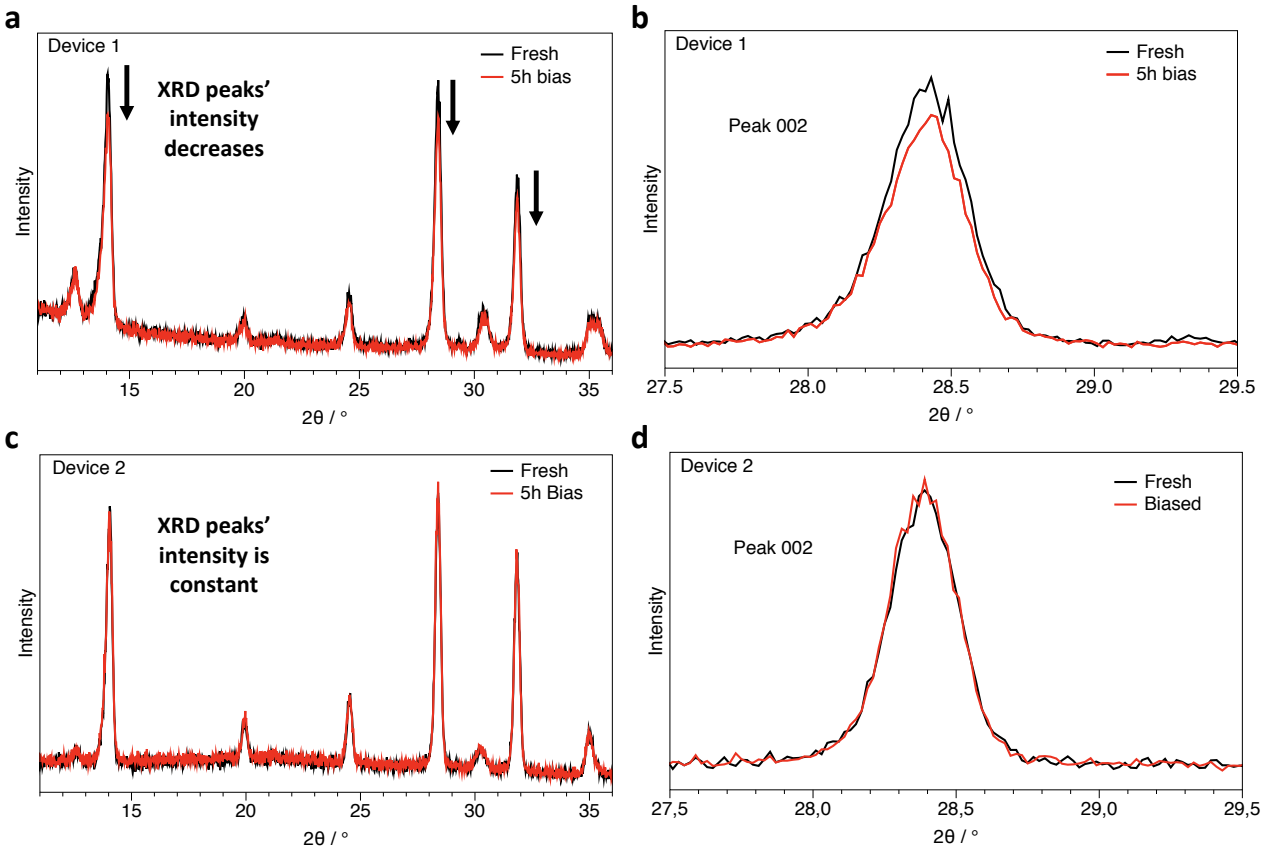

In-situ XRD measurement during biasing of two different devices at 1 V. **a** The XRD pattern of fresh and bias after 5h of device 1 with **b** zoomed in at 28.4° peak, which shows an intensity reduction but no shoulder appearance. **c** The XRD pattern of device 2 biased at 1 V. **d** zoomed in at 28.4° peak, which shows a stable intensity **below** The XRD pattern of different device biased at 1.2 V.

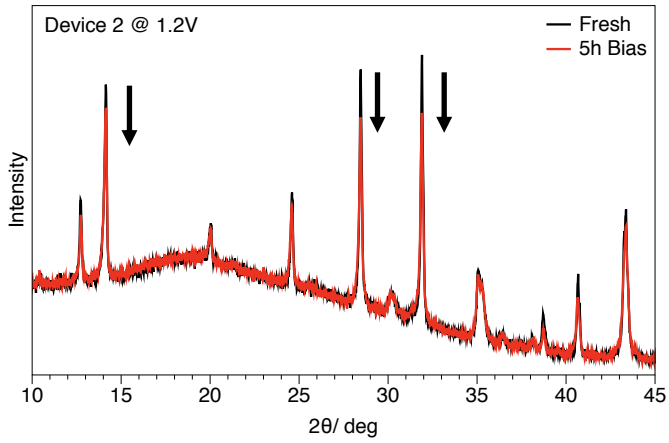

The in-situ XRD experiments were performed also at 1V of biasing. As can be seen in Figure 4d, 1 V did not induce halide segregation, nevertheless, we still saw a loss in J_{SC} and FF as in the case with 1.2 V bias. We measured in situ XRD of two different devices at 1 V. In this condition, we do not observe the loss in XRD peaks intensity for all devices (compare figure SI10a and SI10c). The loss in XRD intensity is more reproducible when biasing at 1.2V (see figure below). This fact suggests

that 1 V might be a threshold value for the amorphization as well as this structural change was likely dependent on the initial device condition. In Figure SI10b, it is shown a representative perovskite's XRD peak showing the decrease of intensity without the appearance of the lower angle shoulder, *i.e.* without halide segregation in agreement with EL stable peak at 1 V.

Figure SI11

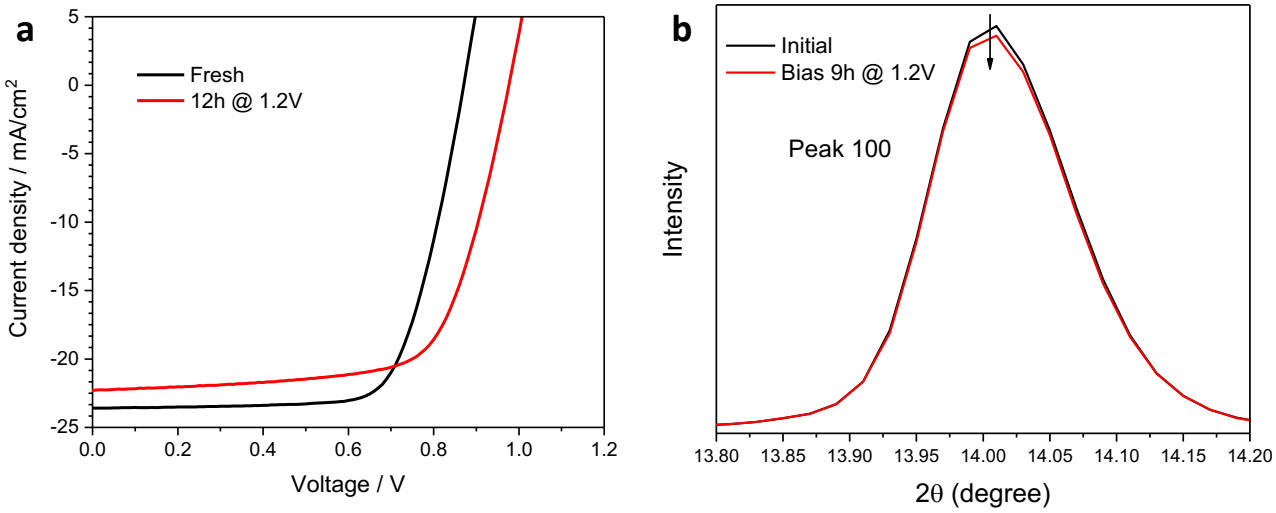

a J-V curves of fresh and biased device using $Cs_{0.1}FA_{0.9}PbI_3$ perovskite. **b** In-situ GIWAXS measurement during biasing at 1.2 V.

To investigate other perovskite system, we chose to use the pure iodide $Cs_{0.1}FA_{0.9}PbI_3$ (CsFA) in the device architecture glass/ITO/NiO/CsFA/C_{60}/BCP/Cu. We observed a similar effect on J-V curve upon biasing with mixed halide system (Figure SI11a). As can be seen in Figure SI11b, the in-situ GIWAXS measurement of this type of device showed some degree of amorphization, however, in lesser degree compared to mixed halide system (around 1.5-2% of integrated intensity loss within the experiment). This together with Figure SI10 indicated that amorphization could occur even without halide segregation but the extent was due to perovskite composition and other factors such as film quality or defect concentration.

Figure SI12

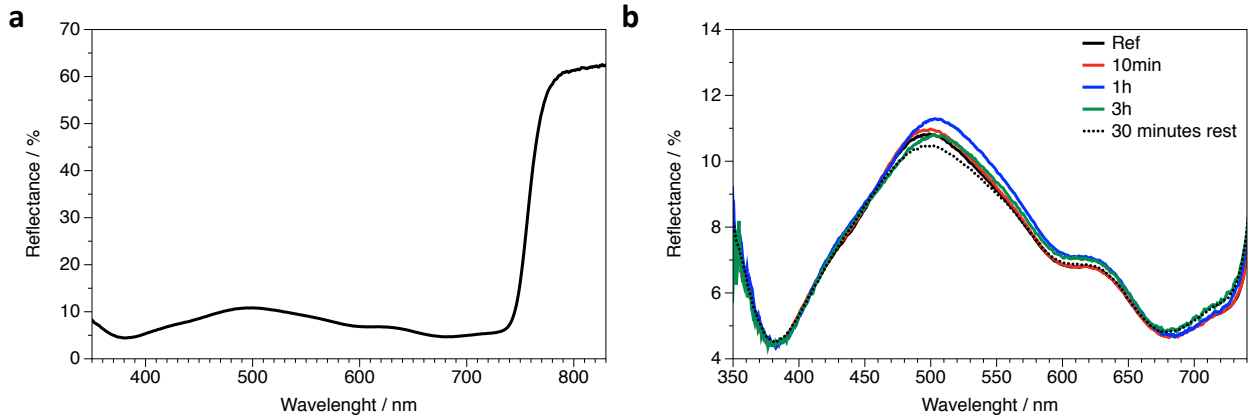

a Reflectance of the full device stack, measured from the glass side. **b** Variation of the reflectance in the 350-750 nm range in the *in-situ* experiment discussed in the main text.

Upon biasing, some slight variation in the complete visible range was observed, as shown above. The decrease of PbI_2 content might be one of the reasons behind changes at short wavelengths, and the selective contacts as well might have an effect.

Figure SI13 PTAA as HSL

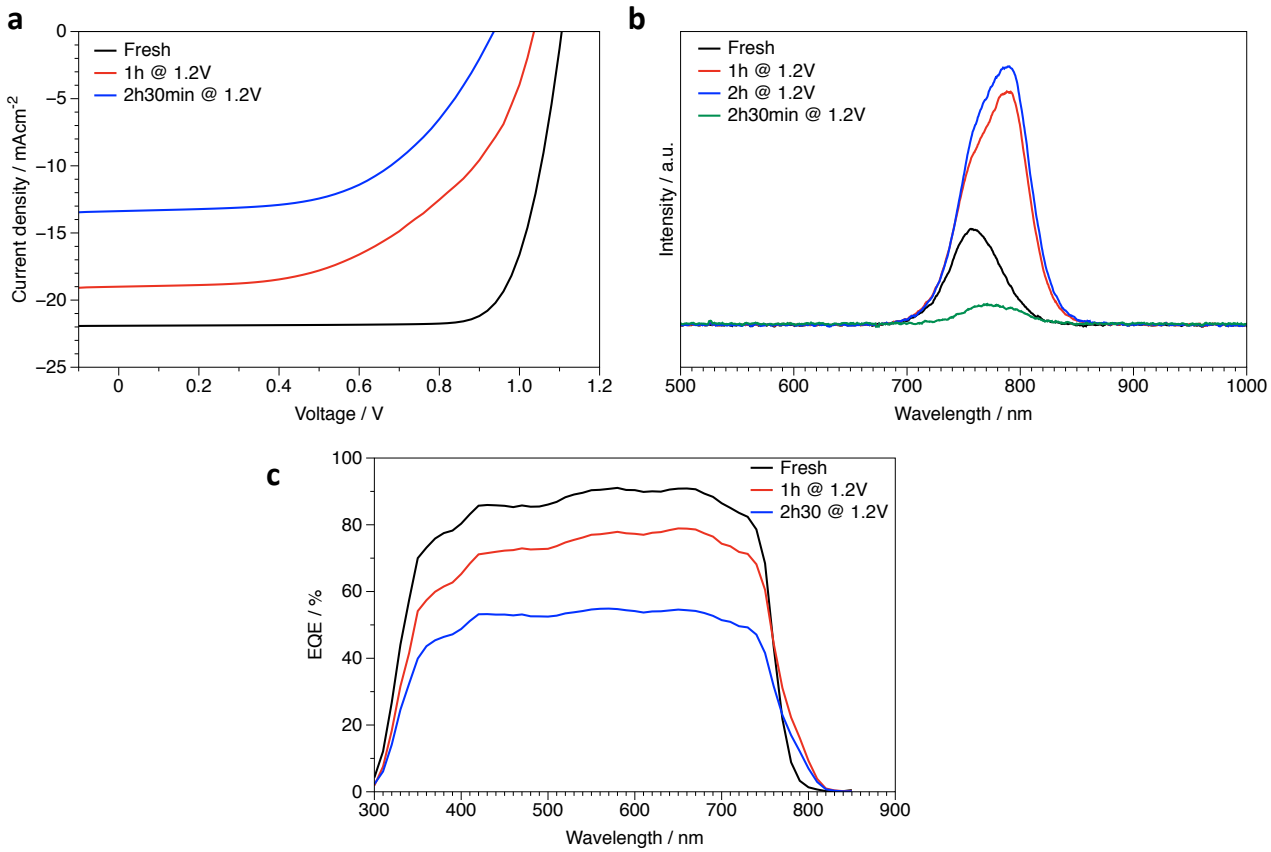

a Effect on JV curves under AM1.5g illumination of the electrical bias (1.2V in dark) on pin PSCs employing PTAA as hole selective layer. **b** Effect of electrical bias on the EL. **c** Effect of the electrical bias on the EQE.

By means of photoelectrical characterizations, we investigated different architectures and configurations of PSCs. We found, as expected, that the degradation path was different depending on the selective contacts. The case of PTAA-based devices was particularly interesting, which was otherwise identical to the NiO-based devices discussed in this work. The PTAA-based devices had efficiency values higher than 19%, which is at the state-of-the-art for p-i-n PSCs (Figure SI1). Nonetheless, the devices appeared overall less stable to electrical bias, hence, the *biased state* after 12h was not presented here (degraded devices yield a straight line in the fourth J-V quadrant). Further, the degradation dynamics was different. Within the first hour (Figure SI10b, c), we found similar changes in EL (increase of efficiency and halide segregation, with the same low band gap species arising) and a similar asymmetric drop in the EQE (larger drop at short wavelengths). Interestingly, the impact on the EQE of the iodide-rich species appears decidedly larger (around 800nm) than in case of NiO-based devices (also in this case a contribution from an enhanced energetic disorder is possible). However, soon after this, a different mechanism emerged for all cells investigated. The

strong decrease in EQE became uniform across the measured wavelength range, *i.e.* not dominant at short wavelengths. We could imagine two different scenarios (not in contradiction to one another) explaining the different degradation routes depending on the hole selective contact. First, PTAA itself might degrade due to ion migration across this very thin layer which has been proven to be a poor ionic barrier.[14] Second, the electric field distribution inside the device, an aspect that has been proven to depend simultaneously on both selective contacts,[15] could change differently as degradation progresses.

Figure SI14

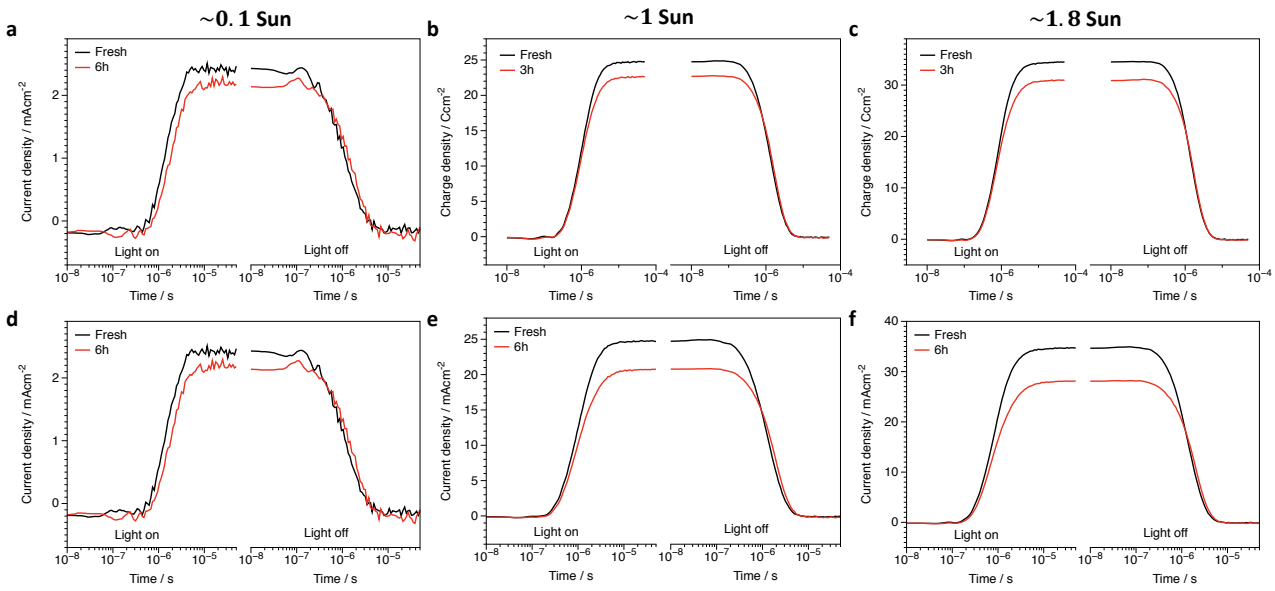

a, b, c) Photocurrent rise and decay obtained in the charge extraction experiments for the fresh device and the same biased for 3h at 1.2 V in dark at different light intensities. **d, e, f)** Photocurrent rise and decay obtained in the charge extraction experiments for the fresh device and the same device biased for 6h at 1.2 V in the dark at different light intensities. In all cases, a decrease of the photocurrent at the plateau of the rise step is obtained upon biasing and a slower extraction of the residual charge is observed when the light is switched off.

Figure SI15

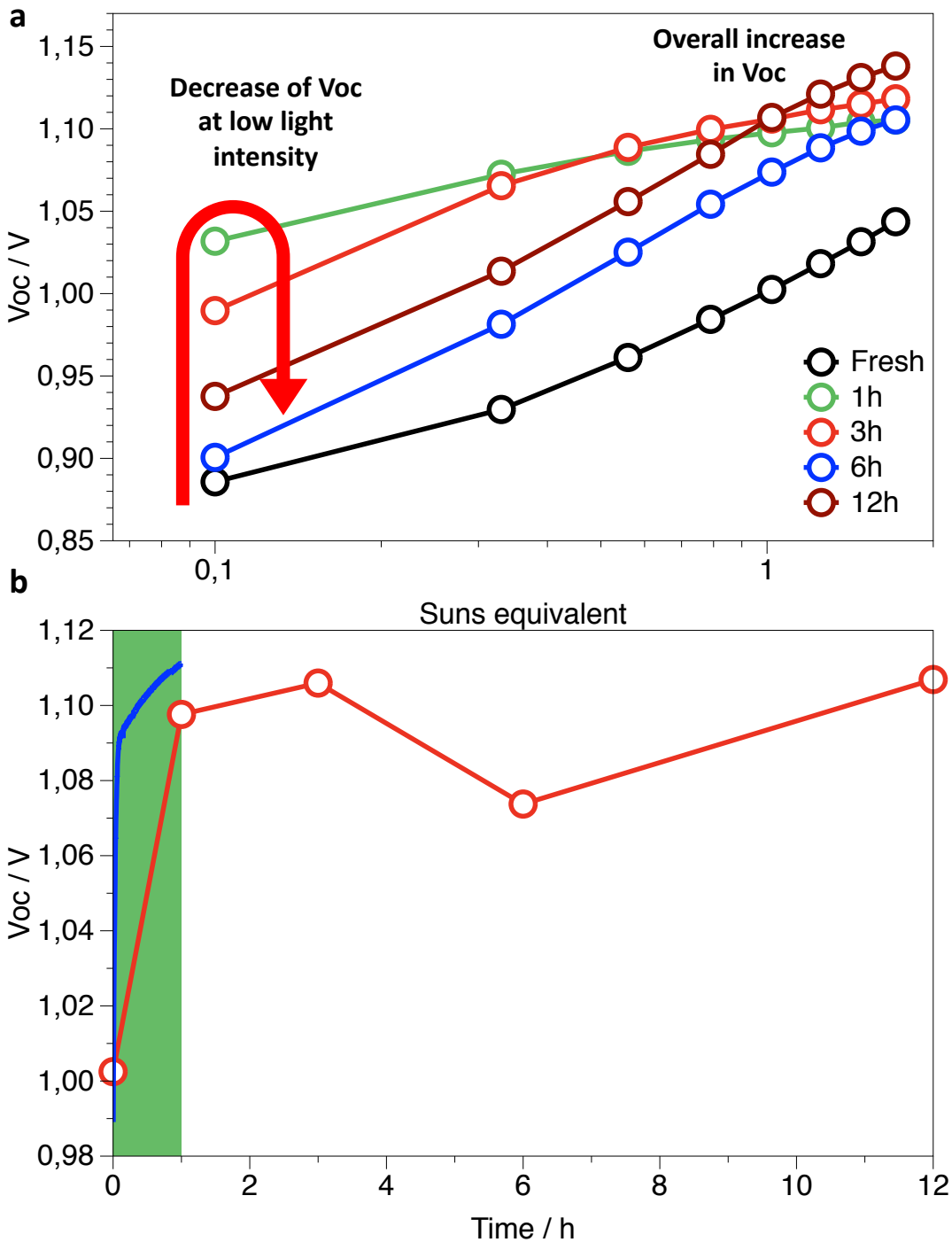

a V_{OC} vs light intensity at different stages of the polarization at 1.2V in dark. **b** V_{OC} at 1 Sun extracted from figure a. In blue it is plotted V_{OC} rise under illumination shown in figure SI2 with the aim of showing that within 1h the plateau of the V_{OC} is already attained.

Note SI2

It is interesting to show that the increase in V_{OC} as obtained from the TPV experiment is non-monotonic over the duration of the stress test. At high illumination (around or above 1 Sun equivalent), the increase in V_{OC} was weakly dependent on the stress duration. This was in line with the plateau in the V_{OC} vs time plot ottained after around 1h and shown in Figure SI3 and Figure SI15b. We could state that the primary mechanism behind the increase of the V_{OC} was already fully effective after less than 1h of poling around the V_{OC} (we expected different kinetics depending on the biasing value, but always faster than the time-scale of investigation in this work). In literature, the rise in V_{OC} upon poling or photo-poling is commonly attributed to the formation of a homogeneous p-i-n junction within the perovskite layer, which reduces the recombination at the interface by minimizing the concentration of electron at the HSL side and electronic holes at the ESL side. This likely apply to our case, as we stated in the main text.

However, at lower illumination levels the situation was different, with the devices biased for more than 1h showing a subsequent V_{OC} decreased. We could not exclude a light-intensity dependent bias induced passivation mechanism. For instance, the charge dynamics at the PbI_2 / perovskite interface has been shown to be fluence dependent.[16] Here, similar concepts could apply to the I-rich perovskite / CsFAMA interface or to the amorphous / crystalline interface. Additionally, the V_{OC} loss at lower light intensity after 1h of biasing might indicate a slight enhancement of the concentration of traps, filled (and so less effective) around 1 Sun but active at lower light intensities.

We believed that it was important to further stress out the anti-correlation between V_{OC} and crystallinity, briefly discussed in the main text. The in-situ XRD data at 1.2 V indicated that a loss of about the 10% of volume of crystalline perovskite could be reached. This would imply a very large defect density over the whole film (10% of unit cells are collapsed). Nonetheless, the V_{OC} remains quite stationary after the first 1-2 hours of poling. A reasonable hypothesis was that the amorphous perovskite was electrically insulated from the crystalline and photoactive one, implying that the amorphous / crystalline interface affected the recombination dynamics. However, unfortunately, very little is known about this interface to propose a convincing atomic mechanism at this stage. Other reasons, which might affect the non-radiative recombination rate, were the halide redistribution after biasing or the improvement of the morphological uniformity of the bulk of the perovskite.

At last, it is interesting that a similar increase in V_{OC} was obtained regardless the halide segregation, pointing to a minor role of this mechanism in defining the device V_{OC} in the biased state. This is to an extent in agreement with the work of Mahesh *et al.*[17]

References

[1] M. V. Khenkin, E. A. Katz, A. Abate, G. Bardizza, J. J. Berry, C. Brabec, F. Brunetti, V. Bulović, Q. Burlingame, A. Di Carlo, R. Cheacharoen, Y.-B. Cheng, A. Colsmann, S. Cros, K. Domanski, M. Dusza, C. J. Fell, S. R. Forrest, Y. Galagan, D. Di Girolamo, M. Grätzel, A. Hagfeldt, E. von Hauff, H. Hoppe, J. Kettle, H. Köbler, M. S. Leite, S. Liu, Y.-L. Loo, J. M. Luther, C.-Q. Ma, M. Madsen, M. Manceau, M. Matheron, M. McGehee, R. Meitzner, M. K. Nazeeruddin, A. F. Nogueira, Ç. Odabaşı, A. Osherov, N.-G. Park, M. O. Reese, F. De Rossi, M. Saliba, U. S. Schubert, H. J. Snaith, S. D. Stranks, W. Tress, P. A. Troshin, V. Turkovic, S. Veenstra, I. Visoly-Fisher, A. Walsh, T. Watson, H. Xie, R. Yıldırım, S. M. Zakeeruddin, K. Zhu, M. Lira-Cantu, *Nat. Energy* **2020**, *5*, 35.

[2] E. H. Anaraki, A. Kermanpur, L. Steier, K. Domanski, T. Matsui, W. Tress, M. Saliba, A. Abate, M. Grätzel, A. Hagfeldt, J.-P. Correa-Baena, *Energy Environ. Sci.* **2016**, *9*, 3128.

[3] S. Rühle, *Sol. Energy* **2016**, *130*, 139.

[4] P. Delugas, C. Caddeo, A. Filippetti, A. Mattoni, *J. Phys. Chem. Lett.* **2016**, *7*, 2356.

[5] C. Caddeo, A. Filippetti, A. Mattoni, *Nano Energy* **2020**, *67*, 104162.

[6] A. Mattoni, A. Filippetti, M. I. Saba, P. Delugas, *J. Phys. Chem. C* **2015**, *119*, 17421.

[7] C. Caddeo, M. I. Saba, S. Meloni, A. Filippetti, A. Mattoni, *ACS Nano* **2017**, acsnano.7b04116.

[8] C. Caddeo, D. Marongiu, S. Meloni, A. Filippetti, F. Quochi, M. Saba, A. Mattoni, *Adv. Mater. Interfaces* **2018**, *6*, 1801173.

[9] Y. Yao, G. Wang, F. Wu, D. Liu, C. Lin, X. Rao, R. Wu, G. Zhou, Q. Song, *RSC Adv.* **2017**, *7*, 42973.

[10] Z. Song, A. Abate, S. C. Watthage, G. K. Liyanage, A. B. Phillips, U. Steiner, M. Graetzel, M. J. Heben, *Adv. Energy Mater.* **2016**, *6*, 1600846.

[11] M. Yuan, L. N. Quan, R. Comin, G. Walters, R. Sabatini, O. Voznyy, S. Hoogland, Y. Zhao, E. M. Beauregard, P. Kanjanaboos, Z. Lu, D. H. Kim, E. H. Sargent, *Nat. Nanotechnol.* **2016**, *11*, 872.

[12] X. Tang, M. van den Berg, E. Gu, A. Horneber, G. J. Matt, A. Osvet, A. J. Meixner, D. Zhang, C. J. Brabec, *Nano Lett.* **2018**, *18*, 2172.

[13] W. Rehman, D. P. McMeekin, J. B. Patel, R. L. Milot, M. B. Johnston, H. J. Snaith, L. M. Herz, *Energy Environ. Sci.* **2017**, *10*, 361.

[14] G. Kakavelakis, I. Paradisanos, B. Paci, A. Generosi, M. Papachatzakis, T. Maksudov, L. Najafi, A. Esaú, D. Rio, G. Kioseoglou, E. Stratakis, F. Bonaccorso, E. Kymakis, **2018**, *1702287*, 1.

[15] I. M. Hermes, Y. Hou, V. W. Bergmann, C. J. Brabec, S. A. L. Weber, *J. Phys. Chem. Lett.* **2018**, *9*, 6249.

[16] A. Merdasa, A. Kiligaridis, C. Rehermann, M. Abdi-Jalebi, J. Stöber, B. Louis, M. Gerhard, S. D. Stranks, E. L. Unger, I. G. Scheblykin, *ACS Energy Lett.* **2019**, *4*, 1370.

[17] S. Mahesh, J. M. Ball, R. D. J. Oliver, D. P. McMeekin, P. K. Nayak, M. B. Johnston, H. J. Snaith, *Energy Environ. Sci.* **2020**, *50*, 675.